SCIENTIFIC PROBLEMS
OF MACHINES OPERATION
AND MAINTENANCE
3 (167) 2011

ANDRZEJ KATUNIN*

The construction of high-order b-spline wavelets and their decomposition relations for fault detection and localisation in composite beams

Key-words

B-spline wavelets, composite beams, faults detection.

Słowa kluczowe

Falki B-splajnowe, belki kompozytowe, detekcja uszkodzeń.

Summary

B-spline scaling functions and wavelets have found wide applicability in many scientific and practical problems thanks to their unique properties. They show considerably better results in comparison to other wavelets, and they are used as well in mathematical approximations, signal processing, image compression, etc. But only the first four wavelets from this family were mathematically formulated. In this work, the author formulates the quartic, quintic and sextic B-spline wavelets and their decomposition relations in explicit form. This allows for the improvement of the sensitivity of fault detection and localisation in composite beams using discrete wavelet transform with decomposition.

* Department of Fundamentals of Machinery Design, Faculty of Mechanical Engineering, Silesian University of Technology, Konarskiego 18A, 44-100 Gliwice, Poland, e-mail: andrzej.katunin@polsl.pl.

Introduction

There is a great interest in the investigation of compactly supported wavelets. This interest is due to the computational capabilities of such wavelets and the wide range of their applications. Forerunners in the development of compactly supported wavelets are Daubechies [1, 2], Cohen, and Feauveau [3]. Spline and B-spline wavelets were also introduced in [4, 5]. The compactly supported orthonormal B-spline wavelets have been found to be a powerful tool in many scientific and practical applications, including mathematical approximations, the finite element method, image processing, and compression and computer-aided geometric design. Thanks to some of their exceptional properties and mathematical simplicity, they are also applied and give very good results in various areas of applied sciences in comparison to other known wavelets.

The last decade demonstrates an augmentation of interest of B-spline wavelets. The scientific group of Lakestani presents several works on solving integral and integro-differential equations using linear B-spline [6], quadratic B-spline [7] and cubic B-spline scaling functions [8]. This wavelet family also found and application in image compression, and the standard of the image compression – JPEG2000 – is based on the B-spline wavelet transform and B-spline factorisation [9]. In problems of the signal processing, B-spline wavelets were used for the development digital filters [10], which show excellent results. Analysing the above-cited works, one can notice a tendency towards the reduction of errors when increasing the order of the B-spline wavelet. In [11] the author presented the possibility of the application B-spline wavelets for diagnostic signal processing. The effectiveness of these wavelets in comparison to other chosen wavelets and the above-mentioned tendency was presented. Therefore, it is necessary to investigate the effectiveness of higher--order B-spline wavelets to improve results, which can be applied in various scientific and technical problems.

There are many methods and techniques for fault detection in problems of technical diagnostics. A large group of these methods are based on signal processing using several transforms (e.g. DFT, STFT) and other techniques (e.g. cepstrum analysis, signal demodulation, etc.), but not all of these techniques can be used for problems of fault detection in the early damage phase [12]. The classic modal analysis may be used only for damage detection, but conclusions about presence of the fault can be made based on the shift of frequency spectrum only, which is a very poor feature in the light of the damage identification problem. Signal processing based on Wavelet Transform (WT) makes it possible to analyse modal shapes in the space domain. Such an analysis is very sensitive to the singularities in the modal shapes, which makes possible the accurate location of a fault, even when the fault is very minimal. It is possible due to the wavelet decomposition algorithm, while one cannot obtain

such information using modal analysis. WT found an application in fault detection in mechanical systems like gearboxes, rolling bearings, rotors, etc., but it can also be applied to structural health monitoring [13, 14]. In [12], the authors show that wavelet analysis makes it possible to detect the type of damage using Continuous WT based on scalogram evaluation. For lightly damaged structures, the authors proposed a method based on Discrete WT, which allows the use of decomposition analysis. In the above-cited work, Daubechies (db8) and Morlet wavelets were used for the approximation.

The problem of fault detection and localisation in beams has been studied in several works. Many of them have been based on simulation results or theoretical models, e.g. [15]. However, fault detection and localisation in experimental research is a more difficult problem, because of the limitation of the number of measuring points and the presence of noise. The authors of [16] presented both the model-based and the experiment-based approach and confirmed the difficulty of fault detection and localisation in real tasks. The authors used the 'symlet4' wavelet for the analysis.

Based on the obtained results in [11] of the comparison of DSD parameters of different wavelets, the author decided to construct higher-order (quartic, quintic and sextic) B-spline wavelets and scaling functions and their decomposition relations. Due to this, using Discrete B-spline WT for fault detection and localisation in composite beams is possible. Pre-notched composite specimens were excited by a random noise signal and displacement was measured using a laser scanning vibrometer. For the signal processing, Discrete B-spline WT was used and fault detection and localisation was evaluated based on the analysis of detailed coefficients by means of the decomposition of the signal. The efficiency of the approximation using B-spline wavelets was compared with other families of orthogonal wavelets. The obtained results indicate the effectiveness of high-order B-spline in fault detection and localisation. Several examples are presented.

Construction of B-spline wavelets

General order B-spline wavelets

The B-spline wavelet can be defined recursively by the convolution [17]:

$$\varphi_m(x) = \int_{-\infty}^{\infty} \varphi_{m-1}\varphi_1(t)dt \tag{1}$$

where

$$\varphi_1(x) = \begin{cases} 0 \text{ for } 0 \le x < 1 \\ 1 \text{ otherwise} \end{cases} \tag{2}$$

The construction of the scaling function of *m*-th order B-spline wavelet is based on the two-scale relation:

$$\varphi_m(x) = \sum_{k=0}^{m} p_k \varphi_m(2x-k) \tag{3}$$

where $\{p_k\}$ is the two-scale sequence and can be expressed as a combination:

$$p_k = 2^{1-m}\binom{m}{k}, \text{ for } 0 \le k < m \tag{4}$$

The two-scale relation for *m*-th order B-spline wavelets is given by:

$$\psi_m(x) = \sum_{k=0}^{3m-2} q_k \varphi_m(2x-k) \tag{5}$$

where

$$q_k = (-1)^k 2^{1-m} \sum_{l=0}^{m} \binom{m}{l} \varphi_{2m}(k-l+1) \tag{6}$$

The decomposition relation for *m*-th order B-spline wavelet is given by:

$$\varphi_m(2x-l) = \sum_k \begin{pmatrix} a_{l-2k}\varphi(x-k) + \\ b_{l-2k}\psi(x-k) \end{pmatrix}, \; l \in Z \tag{7}$$

where decomposition sequences $\{a_k\}$ and $\{b_k\}$ are as follows:

$$a_k = \frac{(-1)^{k+1}}{2} \sum_l q_{-k+2m-2l+1} c_{l,2m} \tag{8}$$

$$b_k = -\frac{(-1)^{k+1}}{2} \sum_l p_{-k+2m-2l+1} c_{l,2m} \tag{9}$$

In (8) and (9) the coefficients sequence $\{c_{k,m}\}$ is presented by *m*-th order Fundamental Cardinal Spline (FCS) function [18]:

$$L_m(x) = \sum_{k=-\infty}^{\infty} c_{k,m} \varphi_m\left(\frac{m}{2} + x - k\right) \tag{10}$$

To obtain the coefficient sequences, the authors of [17] used an analytical relation for B-spline wavelets with order $m < 3$. For higher values of m, obtaining the analytical solutions became very difficult, and for values of m greater than 5, it is impossible in the light of Abel-Ruffini theorem. Therefore, the analytical formula was omitted here. Another way of obtaining the coefficient sequences is to form the bi-infinite system of equations [18] as follows:

$$\sum_{k=-\infty}^{\infty} c_{k,m}\varphi_m\left(\frac{m}{2}+j-k\right)=\delta_{j,0},\quad j\in Z \tag{11}$$

The explicit form of (11) for $m = 2$ can be written as (cf. [17]):

$$\begin{bmatrix} \ddots & & & & & & \\ & \varphi_4(1) & \varphi_4(2) & \varphi_4(3) & & & \\ & & \varphi_4(1) & \varphi_4(2) & \varphi_4(3) & & \\ 0 & & & & & & \ddots \end{bmatrix} \begin{bmatrix} \vdots \\ c_{-2} \\ c_{-1} \\ c_0 \\ c_1 \\ c_2 \\ \vdots \end{bmatrix} = \begin{bmatrix} \vdots \\ 0 \\ 1 \\ 0 \\ \vdots \end{bmatrix} \tag{12}$$

The coefficients sequence $\{c_{k,m}\}$ is infinite for $m \geq 3$, so that (10) does not vanish identically outside any compact set. However, these coefficients decay to zero exponentially fast as $k \to \infty$, which implies decaying to zero of (10) as $x \to \pm\infty$.

Quartic B-spline wavelet (m = 5)

Quartic B-spline $\varphi_5(x)$ scaling function is given by the next recurrence relation:

$$\varphi_5(x)=\begin{cases} \dfrac{x^4}{24} \\ -\dfrac{x^4}{6}+\dfrac{5x^3}{6}-\dfrac{5x^2}{4}+\dfrac{5x}{6}-\dfrac{5}{24} \\ \dfrac{x^4}{4}-\dfrac{5x^3}{2}+\dfrac{35x^2}{4}-\dfrac{25x}{2}+\dfrac{155}{24} \\ -\dfrac{x^4}{6}+\dfrac{5x^3}{2}-\dfrac{55x^2}{4}+\dfrac{65x}{2}-\dfrac{655}{24} \\ \dfrac{x^4}{24}-\dfrac{5x^3}{6}+\dfrac{25x^2}{4}-\dfrac{125x}{6}+\dfrac{625}{24} \end{cases} \tag{13}$$

where the support changes in the range [0,*m*] with step 1 referring to the property of B-spline scaling functions. Two-scale sequences $\{p_5\}$ and $\{q_5\}$ are presented in (14) and (15). Based on them, two-scale relations for $\varphi_5(x)$ and $\psi_5(x)$ can be constructed using (3) and (5), respectively.

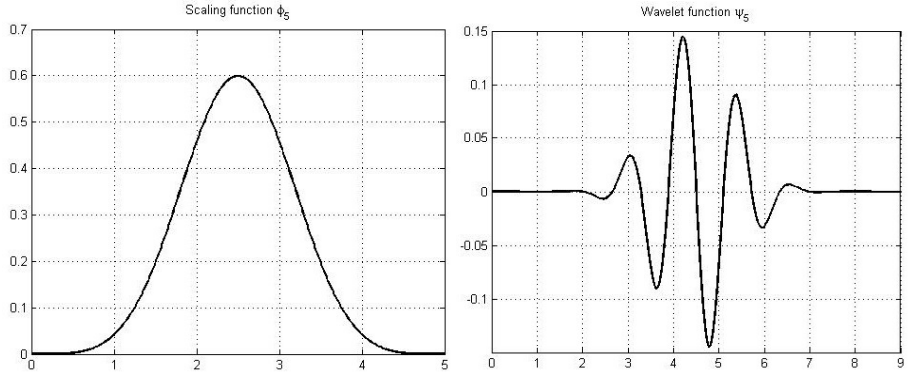

Fig. 1. Scaling and basic functions of quartic B-spline wavelet
Rys. 1. Funkcja skalująca i bazowa falki B-splajnowej rzędu 5

Decomposition sequences were calculated using (8), (9) and (12). For quartic B-spline wavelet some of them are presented in Tab. 1.

$$\{p_5\}=\left\{\frac{1}{16};\frac{5}{16};\frac{5}{8};\frac{5}{8};\frac{5}{16};\frac{1}{16}\right\} \tag{14}$$

$$\{q_5\}=\left\{\begin{array}{l}\frac{1}{5806080};-\frac{169}{1935360};\frac{2141}{725760};\\ -\frac{5197}{181440};\frac{149693}{1161216};-\frac{54289}{165888};\\ \frac{74339}{145152};-\frac{74339}{145152};\frac{54289}{165888};\\ -\frac{149693}{1161216};\frac{5197}{181440};-\frac{2141}{725760};\\ \frac{169}{1935360};\frac{1}{5806080}\end{array}\right\} \tag{15}$$

Table 1. Quartic B-spline decomposition sequences
Tabela 1. Współczynniki dekompozycji dla falki B-splajnowej rzędu 5

$\lvert k\rvert$	a_{k-2}	b_{k-2}
0	0.27944	0.26081
1	-0.03765	-0.1238
2	-0.48157	-0.44529
3	-0.05206	0.08078
4	0.87419	0.73019
5		-0.20474
6		-1.15096
7	⋮	0.54171
8		1.59650
⋮		⋮

Quintic B-spline wavelet (m = 6)

Let us go to the next example $\varphi_6(x)$ given by

$$\varphi_6(x)=\begin{cases}\dfrac{x^5}{120}\\ -\dfrac{x^5}{24}+\dfrac{x^4}{4}-\dfrac{x^3}{2}+\dfrac{x^2}{2}-\dfrac{x}{4}+\dfrac{1}{20}\\ \dfrac{x^5}{12}-x^4+\dfrac{9x^3}{2}-\dfrac{19x^2}{2}+\dfrac{39x}{4}-\dfrac{79}{20}\\ -\dfrac{x^5}{12}+\dfrac{3x^4}{2}-\dfrac{21x^3}{2}+\dfrac{71x^2}{2}-\dfrac{231x}{4}+\dfrac{231}{4}\\ \dfrac{x^5}{24}-x^4+\dfrac{19x^3}{2}-\dfrac{89x^2}{2}+\dfrac{409x}{4}-\dfrac{1289}{20}\\ -\dfrac{x^5}{120}+\dfrac{x^4}{4}-3x^3+18x^2-54x+\dfrac{324}{5}\end{cases} \tag{16}$$

and shown in Fig. 2. Two-scale sequences $\{p_6\}$ and $\{q_6\}$ are given by (17) and (18), respectively. Because of the symmetry of $\{q_6\}$, only the half sequence was presented.

$$\{p_6\}=\left\{\frac{1}{32};\frac{3}{16};\frac{15}{32};\frac{5}{8};\frac{15}{32};\frac{3}{16};\frac{1}{32}\right\} \tag{17}$$

$$\{q_6\}=\left\{\begin{array}{l}\dfrac{1}{1277337600};-\dfrac{1021}{638668800};\\ \dfrac{1249}{9676800};-\dfrac{314487}{127733760};\\ \dfrac{6322333}{319334400};-\dfrac{6127141}{70963200};\\ \dfrac{74131711}{319334400};-\dfrac{10504567}{25546752};\\ \dfrac{21112517}{42577920};\ldots\end{array}\right\} \tag{18}$$

Decomposition sequences for quintic B-spline are given in Tab. 2.

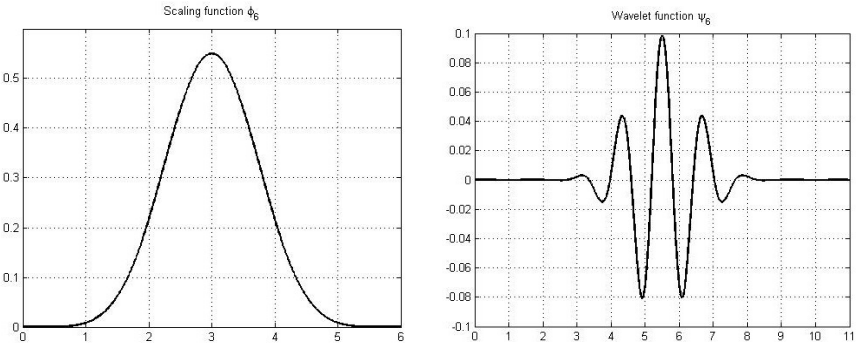

Fig. 2. Scaling and basic functions of quintic B-spline wavelet
Rys. 2. Funkcja skalująca i bazowa falki B-splajnowej rzędu 6

Table 2. Quintic B-spline decomposition sequences
Tabela 2. Współczynniki dekompozycji dla falki B-splajnowej rzędu 6

k	a_{k-2}	b_{k-2}
0	0.29214	-0.24695
1	0.29398	-0.35522
2	-0.41198	0.46725
3	-0.55802	0.48370
4	0.48972	-0.77160
5	1.24143	-0.65901
6	⋮	1.22365
7		0.82492
8		-1.91952
9		-0.69623
10		2.84275
⋮		⋮

Sextic B-spline wavelet

The last presented wavelet scaling function $\varphi_7(x)$ is given by the following:

$$\varphi_7(x)=\begin{cases}\dfrac{x^6}{720}\\ -\dfrac{x^6}{120}+\dfrac{7x^5}{120}-\dfrac{7x^4}{48}+\dfrac{7x^3}{36}-\dfrac{7x^2}{48}+\dfrac{7x}{120}-\dfrac{7}{120}\\ \dfrac{x^6}{48}-\dfrac{7x^5}{24}+\dfrac{77x^4}{48}-\dfrac{161x^3}{36}+\dfrac{329x^2}{48}+\dfrac{133x}{24}-\dfrac{1337}{720}\\ -\dfrac{x^6}{36}+\dfrac{7x^5}{12}-\dfrac{119x^4}{24}+\dfrac{196x^3}{9}-\dfrac{1253x^2}{24}+\dfrac{196x}{3}+\dfrac{12089}{360}\\ \dfrac{x^6}{48}-\dfrac{7x^5}{12}+\dfrac{161x^4}{24}-\dfrac{364x^3}{9}+\dfrac{3227x^2}{24}-\dfrac{700x}{3}-\dfrac{59591}{360}\\ -\dfrac{x^6}{120}+\dfrac{7x^5}{24}-\dfrac{203x^4}{48}+\dfrac{1169x^3}{36}-\dfrac{6671x^2}{48}-\dfrac{7525x}{24}-\dfrac{208943}{720}\\ \dfrac{x^6}{720}-\dfrac{7x^5}{720}+\dfrac{49x^4}{48}-\dfrac{343x^3}{36}+\dfrac{2401x^2}{48}-\dfrac{16807x}{120}+\dfrac{117649}{720}\end{cases} \tag{19}$$

and two-scale sequences are given by (20) and (21). Because of the anti-symmetry of $\{q_7\}$, only the half sequence was presented. Graphical interpretation of $\varphi_7(x)$ and $\psi_7(x)$ is presented in Fig. 3. Decomposition sequences are tabulated in Tab. 3.

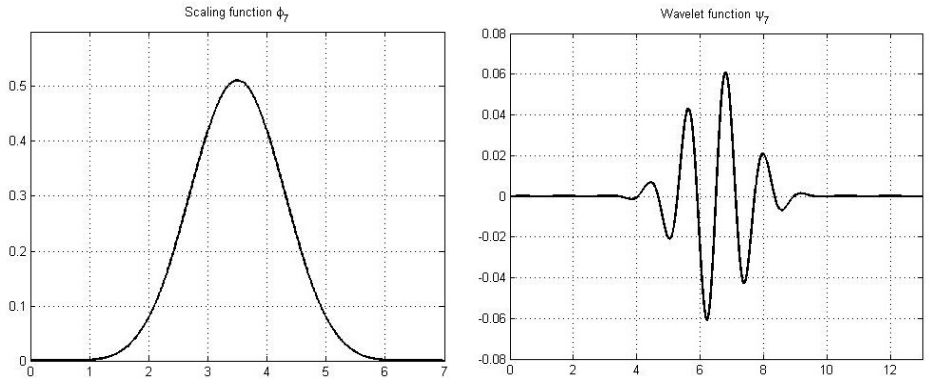

Fig. 3. Scaling and basic functions of sextic B-spline wavelet
Rys. 3. Funkcja skalująca i bazowa falki B-splajnowej rzędu 7

$$\{p_7\}=\left\{\frac{1}{64};\frac{7}{64};\frac{21}{64};\frac{35}{64};\frac{35}{64};\frac{21}{64};\frac{7}{64};\frac{1}{64}\right\} \tag{20}$$

$$\{q_7\}=\left\{\begin{array}{l}\dfrac{1}{398529331200};-\dfrac{1637}{79705866240};\\ \dfrac{170777}{44281036800};-\dfrac{11212661}{79705866240};\\ \dfrac{193344049}{99632332800};-\dfrac{456405947}{33210777600};\\ \dfrac{33355811}{569327616};-\dfrac{2338911899}{14233190400};\\ \dfrac{605806759}{1897758720};-\dfrac{12583103921}{28466380800};\ldots\end{array}\right\} \tag{21}$$

Table 3. Sextic B-spline decomposition sequences
Tabela 3. Współczynniki dekompozycji dla falki B-splajnowej rzędu 7

$\lvert k\rvert$	a_{k-2}	b_{k-2}
0	0.05808	-0.09463
1	0.57369	0.73914
2	-0.00377	-0.02005
3	-0.85444	-1.08620
4	-0.23318	0.16139
5	1.22519	1.54667
6		-0.37510
7		-2.14425
8		0.77637
9	⋮	2.82425
10		-1.62267
11		-3.18547
⋮		⋮

Notice that, in Tables 1 through 3, decomposition sequences were limited to unique values. In the case of $\{a_k\}$, there is symmetry of the sequence; therefore, only half of it is presented. In the case of $\{b_k\}$, the sequence is symmetrical for even *m* and anti-symmetrical for odd *m*.

Comparative analysis of approximation effectiveness of some (semi)-orthogonal wavelet families

The evaluation of the approximation effectiveness can be executed using the degree of scalogram density (DSD) parameter. In technical diagnostics, DSD was used by A. Timofiejczuk [19]. DSD is a statistical scalar parameter, which

is based on the normalisation of the set of wavelet coefficients from the scalogram, their filtering for some non-zero threshold and determination using the following dependence:

$$DSD = 1 - \frac{N}{L} \tag{22}$$

where N denotes the number of wavelet coefficients greater than threshold value and L is the number of all wavelet coefficients.

In this section, we will compare DSD for various wavelet families for three types of signals, which most frequently occur in diagnostic signal processing: the harmonic one, the harmonic with variable frequency (chirp), and the triangular pulse. One may consider only orthogonal or semi-orthogonal (e.g. B-spline) wavelets, because Discrete WT is possible only using such wavelets.

Wavelets and their decomposition relations from Section 2 were implemented into MATLAB®. Then, the DSD test was performed with a threshold value of 0.01, a scale parameter of 1–256 and time of 2 s with sampling rate 0.0001 s. The obtained results are presented in Figs. 4 through 6 for investigated types of signals. Note, that first-order Daubechies and B-spline wavelets are identical to the Haar wavelet.

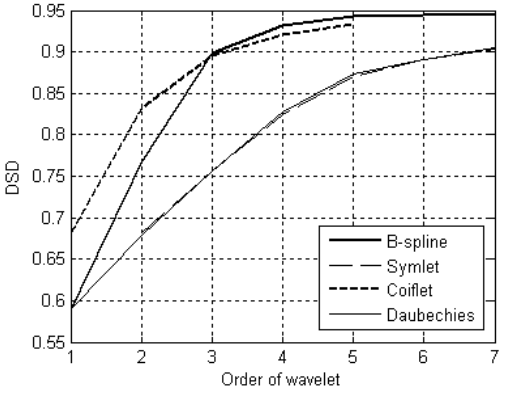

Fig. 4. DSD parameter for the harmonic component
Rys. 4. Stopień zagęszczenia skalogramu dla składowej harmonicznej

As it can be observed, the B-spline wavelet gives the best DSD parameter for each considered type of signal. In cases of harmonic components, DSD reveals asymptotic convergence to unity with the increase in the order of the wavelet. For harmonic components, the growth of DSD is stabilised after the fifth order; therefore, the construction of B-spline wavelets with an order higher than seventh is not profitable. Analysing DSD values in Fig. 6, one can conclude

that DSD has a decreasing tendency with the increase in the order of the wavelet. However, values of DSD are very good for all considered orders of B-spline wavelets and the changes of DSD are minor, i.e. B-spline wavelets can be used in diagnostic signal processing for pulse components as well.

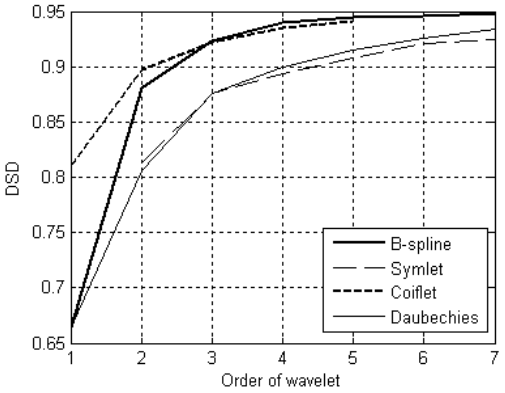

Fig. 5. DSD parameter for the harmonic component with variable frequency
Rys. 5. Stopień zagęszczenia skalogramu dla składowej harmonicznej ze zmienną częstotliwością

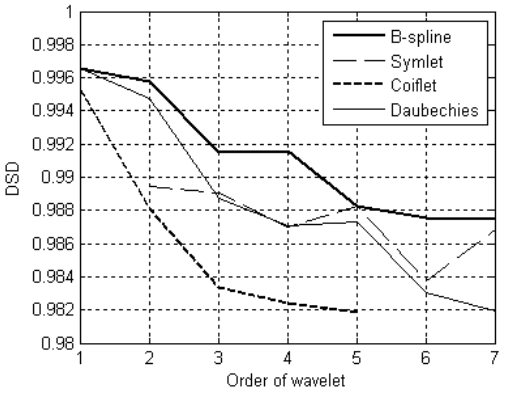

Fig. 6. DSD parameter for the pulse component
Rys. 6. Stopień zagęszczenia skalogramu dla składowej impulsowej

Fault detection in composite beams

Specimens preparation and experimental setup

The specimens were manufactured from 24-layered glass fiber-reinforced epoxy laminate in the form of unidirectional impregnated fibers. The configuration of the specimens was selected in order to achieve transversal

isotropic properties. The structural formula and material properties of the specimens can be found in [20]. The dimensions of the specimens were defined as follows: length L = 250 mm, width W = 25 mm and thickness H = 5.28 mm. Three specimens (one sound and two pre-notched) were considered. Notches, whose depth h is 1 mm, were located at the distance l of 0.28L and 0.6L, respectively. Fig. 7 shows the scheme of the investigated specimens.

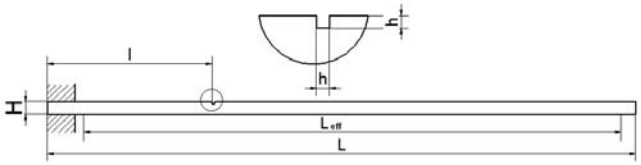

Fig. 7. Dimensions of the specimens
Rys. 7. Wymiary próbek

The specimens were clamped on one side at length of 0.08L. For the excitation, the random noise signal was generated and amplified by a power amplifier and exerted to the beam through the TIRA TV-51120 modal shaker. For measurements, Laser Doppler Vibrometers (LDV) were used, which provided highly precise values. The scanning LDV (Polytec PSV-400) was used for sensing the response signal of the beam, and a second LDV (Polytec PDV-100) was used for achieving the reference signal. Measurements were provided in the bandwidth of 1 to 3200 Hz with a sample frequency of 8192 Hz. On the effective measurement length L_{eff} of 215 mm (from 0.1L to 0.96L), a line with 44 measurement points was defined. The interval between points was 5 mm. The experimental setup is presented in Fig. 8.

Fig. 8. Experimental setup
Rys. 8. Stanowisko badawcze

Then, the testing of above-mentioned specimens was carried out. Frequency response functions obtained during the modal analysis were stored and, based on them, the natural frequencies and modal shapes were determined. The displacement data for selected modal shapes of resonant vibrations were acquired and exported to MATLAB®.

Analysis and experimental results

In obtained frequency spectra of the first four natural modes of vibration were selected and considered in the analysis. Then, the discrete wavelet transform with high-order B-spline wavelets was performed. Preliminary analysis indicates that symmetric B-spline wavelets give better results in the decomposition process; therefore, the quintic B-spline wavelet was used in the next analysis. After decomposition, detail coefficients of signals for each case were investigated. Additionally, the soft threshold filtering was conducted for de-noising detail coefficients. Exemplary detail coefficients before and after de-noising are shown in Fig. 9. After these operations, zero-value detail coefficients for healthy specimen were obtained. Therefore, the graphical presentation of detail coefficients was omitted for this specimen. The approximation and detail coefficients of pre-notched specimens are depicted in Fig. 10. The first column contains approximations (Y-axis – approximation coefficient). The second column contains detail coefficients for the specimen with the notch at 0.6*L* (Y-axis – details coefficient). The third column contains detail coefficients for the specimen with the notch at 0.28*L* (Y-axis – details coefficient). For all, the X-axis is the distance, *L* [mm].

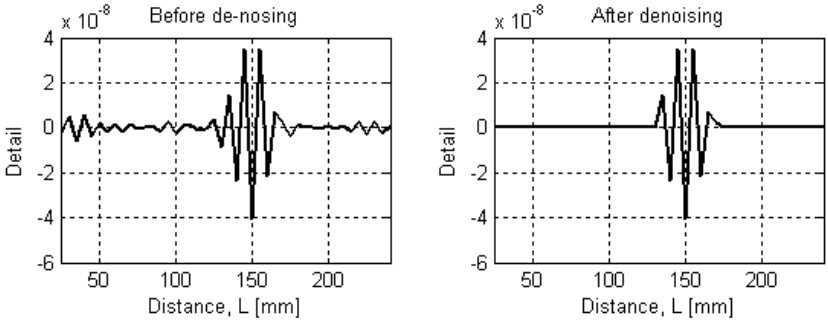

Fig. 9. De-noising of the detail for the specimen with the notch at 0.6L for the 1st mode shape
Rys. 9. Odszumienie współczynników detalu dla próbki z pęknięciem w 0,6L dla pierwszej postaci własnej

As seen in Fig. 9, the de-noising operation allows one to remove the measurement noise and to present changes in the detail coefficients. However, because of the high-order of the applied wavelet and the consequently larger number of vanishing moments of this wavelet, fault localisation became more

difficult and detail coefficients could not be used to visualise the exact location of the fault (see Figs. 10e–g and Figs. 10k–l). On the other hand, the small number of vanishing moments of the wavelet could influence the accuracy of the decomposition process. By analysing details from the decomposition by means of the geometry of the wavelet, one can notice that the fault localisation can be provided by the evaluation of the highest value of the de-noised detail coefficients.

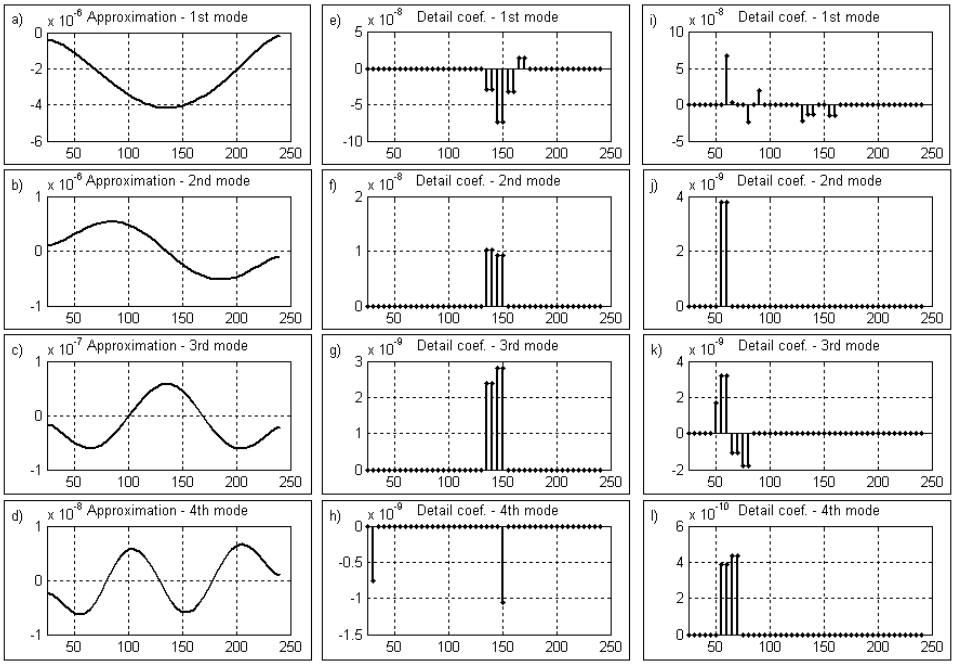

Fig. 10. Decomposition of measured signals for four mode shapes of beams
Rys. 10. Dekompozycja sygnałów pomiarowych dla czterech postaci własnych belek

Discussion

In the present work, high-order B-spline wavelets were proposed. The analytical formulation of quartic, quintic, and sextic B-spline wavelets and their decomposition relations were presented. The comparative analysis of wavelets, which could be used for Discrete WT, indicates the highest effectiveness of B-spline wavelets, especially for higher orders. The construction of wavelets with an order higher than 7 is not well grounded. The analytical formulation of these wavelets and their decomposition relations could be difficult, but the practical application of them will also be limited because of the increasing the number of vanishing moments and the effective support.

One of presented wavelets, the quintic B-spline wavelet, was applied for fault detection and localisation in composite beams. The selection of the appropriate wavelet to such analysis is crucial. However, in analysis, one can noticed the effectiveness of the above-mentioned wavelet. As previously shown, fault localisation using a decomposition procedure with B-spline wavelets is possible after detail coefficient de-noising and gives precise results. The accuracy of the damage localisation is directly dependent on the number of measurement points. With a higher number of measurement points, the displacements of a given modal shape can be determined more accurately.

An application of high-order B-spline wavelets is not only limited to the problem presented above. They can also be used for numerical solving of differential equations, where the wavelet scaling function is a differential operator. Moreover, they could find an application in structural health monitoring of complex problems, pattern recognition problems, signal processing in biomedical applications, etc.

In further works, the use of the presented wavelets for detection and localisation of faults in multi-damaged structures will be investigated. An additional task will be the evaluation of structural life assessment based on detail coefficients.

References

[1] Daubechies I.: Orthonormal bases of compactly supported wavelets, Communications on Pure and Applied Mathematics 41, 1988, pp. 909–996.
[2] Daubechies I.: Ten lectures on wavelets, Society of Industrial and Applied Mechanics (SIAM), Philadelphia, PA, 1992.
[3] Cohen A., Daubechies I., Feauveau J.-C.: Biorthogonal bases of compactly supported wavelets, Communications on Pure and Applied Mathematics 45, 1992, pp. 485–560.
[4] Chui C.K.: An introduction to wavelets, Academic Press, 1992.
[5] Chui C.K., Wang J.: A general framework of compactly supported splines and wavelets, Journal of Approximation Theory 71, 1992, pp. 54–68.
[6] Lakestani M., Razzaghi M., Dehghan M.: Solution of nonlinear Fredholm-Hammerstein integral equations by using semiorthogonal spline wavelets, Mathematical Problems in Engineering 1, 2005, pp. 113–121.
[7] Malenejad K., Aghazadeh N.: Solving nonlinear Hammerstein integral equations by using B-spline scaling functions, Proc. of the World Congress of Engineering, London, 2009.
[8] Dehghan M., Lakestani M.: Numerical solution of Ricatti equation using the cubic B-spline scaling functions and Chebyshev cardinal functions, Computer Physics Communications 181(5), 2010, pp. 957–966.
[9] Taubman D.S., Marcellin M.W.: JPEG2000: image compression fundamentals, standards and practice, Kluwer Academic Publishers, 2002.
[10] Samadi S., Achmad M.O., Swamy M.N.S.: Characterization of B-spline digital filters, IEEE Transactions on Circuits and Systems 51(4), 2004, pp. 808–816.
[11] Katunin A., Korczak A.: The possibility of application of B-spline family wavelets in diagnostic signal processing, Acta Mechanica et Automatica 3(4), 2009, pp. 43–48.
[12] Katunin A., Moczulski W.: Faults detection in composite layered structures using wavelet transform, Diagnostyka 1(53), 2010, pp. 27–32.

[13] Hou Z., Noori M., Amand R.: Wavelet-based approach for structural damage detection, J. Eng. Mech., 126(7), 2000, pp. 677–683.
[14] Moyo P., Brownjohn J.M.W.: Detection of anomalous structural behaviour using wavelet analysis, Mechanical Systems and Signal Processing 16(2-3), 2002, pp. 429–445.
[15] Douka E., Loutridis S., Trochidis A.: Crack identification in plates using wavelet analysis, Journal of Sound and Vibration 270, 2004, pp. 279–295.
[16] Zhong S., Oyadiji S.O.: Crack detection in simply supported beams using stationary wavelet transform of modal data, Structural Control and Health Monitoring 18(2), 2010, pp. 169–190.
[17] Ueda M., Lodha S.: Wavelets: an elementary introduction and examples, University of California, Santa Cruz, 1995.
[18] Chui C.K.: On cardinal spline wavelets, Wavelets and their applications, Jones and Bartlett, Boston, 1992, pp. 419–438.
[19] Timofiejczuk A.: Methods of analysis of non-stationary signals, Silesian University of Technology Publishing House, Gliwice, 2004 [in Polish].
[20] Katunin A., Moczulski W.: The conception of a methodology of degradation degree evaluation in laminates, Eksploatacja i Niezawodnosc – Maintenance and Reliability 41, 2009, pp. 33–38.

Konstrukcja falek b-splinowych wyższych rzędów i ich zależności dekompozycji dla detekcji i lokalizacji uszkodzeń w belkach kompozytowych

S t e s z c z e n i e

B-splajnowe funkcje skalujące i falki znajdują szerokie zastosowanie w wielu zagadnieniach naukowych i praktycznych dzięki ich wyjątkowym właściwościom. Pokazują one znacznie lepsze wyniki w porównaniu z innymi falkami i są z powodzeniem stosowane w matematycznych aproksymacjach, przetwarzaniu sygnałów, kompresji obrazów itd. Ale tylko pierwsze cztery falki z tej rodziny zostały sformułowane matematycznie. W niniejszej pracy autor sformułował falki B-splajnowe wyższych rzędów i ich zależności dekompozycji w postaci jawnej. Pozwalają one na zwiększenie dokładności przy detekcji i lokalizacji uszkodzeń w belkach kompozytowych z zastosowaniem dyskretnej transformacji falkowej z dekompozycją.